IEEE Access
Multidisciplinary | Rapid Review | Open Access Journal

Received May 20, 2019, accepted June 23, 2019, date of publication June 27, 2019, date of current version August 7, 2019.

Digital Object Identifier 10.1109/ACCESS.2019.2925465

Three Dimensional Auto-Alignment of the ICSI Pipette

FERHAT SADAK, MOZAFAR SAADAT, (Senior Member, IEEE), AND AMIR M. HAJIYAVAND
Medical Robotic Group, Automation and Intelligent Manufacturing (AIM) Laboratory, Department of Mechanical Engineering, School of Engineering, University of Birmingham, Birmingham B15 2TT, U.K.

Corresponding author: Amir M. Hajiyavand (a.hajiyavand@bham.ac.uk)

This work was supported in part by the U.K. Medical Research Council (MRC).

ABSTRACT Intracytoplasmic sperm injection (ICSI) is an assisted reproductive technology used in infertility treatment, where a single sperm is selected and immobilized using a glass injection pipette and is inserted directly into the cytoplasm of an oocyte under the microscope. Auto-alignment of the injection pipette is a prerequisite for any proposed automated oocyte injection procedure. In this paper, an auto-alignment procedure has been proposed. This technique requires the positioning of the injection and holding pipettes in the three orthogonal axes under microscopy which is complex. The existing proposed methods are system-specific and require appropriate algorithms. In this paper, 12 commonly used focusing algorithms were evaluated to verify the optimal one for the ICSI application. These algorithms were assessed by measuring focusing accuracy, range, the number of false maxima, and the width of the curve. The focus level for each pipette is calculated by the algorithm using focus measure functions (FMA). The Fibonacci search algorithm is employed for controlling the z-axis of the motorized stage to obtain the focal plane of the injection and holding pipette. The experimental results verified that the Brenner gradient has demonstrated the highest overall performance for injection pipette focalization, while the energy of gradient has presented a highest overall performance for holding pipette focalization.

INDEX TERMS Intracytoplasmic sperm injection (ICSI), autofocusing, computer vision, focus measurement algorithm, Fibonacci search.

I. INTRODUCTION

Intracytoplasmic sperm injection (ICSI), first presented in 1992, is an assisted reproductive technology in which a single spermatozoon is injected into the oocyte using a glass injection micropipette [1]. There has been considerable demand to automate the ICSI processes to enhance their success and survival rate [2]–[6]. This is because the manual operation is conducted by a trained embryologist, relying on the visual information through the microscope. However, manual operation is time-consuming and may cause oocyte damage, with the consequence of a low success rate. To automate the oocyte injection task, the injection pipette must be aligned with the holding pipette at a desired position prior to the ICSI procedure to ensure the correct injection. This is key to accurately conducting the fully automated ICSI process and increasing system efficiency. This is because the tip of the injection and holding pipette can be easily damaged during the ICSI process if the injection pipette is not aligned correctly to the holding pipette. The micropipettes could fail to penetrate the zona pellucida or oolemma membrane of the oocyte [7]. This would cause a serious injury to the oocyte membrane or require a replacement of the micropipettes. Therefore, this makes accurate focusing a necessity.

Autofocusing can be examined using passive and active methods depending on the way of measuring the distance between the lens and the object. Active autofocusing measures the distance externally using ultrasonic or infrared waves, whilst passive autofocusing measures the sharpness of the images captured at different focal positions and finds the peak point of the obtained focus curve [8]. Active autofocusing demonstrates an effective sensing mechanism under different lighting conditions. However, such a sensing technique may struggle to focus well through glass due to high infrared or ultrasound reflectivity [9]. Passive auto-focusing relies on the image information and it is not essential to consider

The associate editor coordinating the review of this manuscript and approving it for publication was Vishal Srivastava.

reflectivity since there is no external sensor included. It also decreases the cost markedly. Consequently, image-based passive auto-focusing will be discussed in this paper since it does not require any additional device such as a range finding sensor as in active autofocusing [10].

A variety of focusing algorithms have been proposed such as Brenner gradient, Tenengrad gradient, and Energy gradient to adjust the experimental sample in an accurate position in the focal zone of the microscope [11]–[13]. Since the injection and holding pipette presents a unimodal focus curve, focusing algorithm methods can be utilized. However, selection of an appropriate focus algorithm for a fully automated ICSI process remains deficient in previous researches since the selection of the optimal autofocusing algorithm greatly depends on the specific application [14]. Previous literature has discussed finding the focal distance of the micro-objects as it is a challenging task in micro applications where the depth of focus is a crucial parameter and plays an essential role.

Template matching is a technique in the field of computer vision for searching a portion of a sourced image which matches a template image obtained in advance. Template matching technique has recently been proposed for an automatic oocyte injection process to find the depth of micropipettes [15]. Based on the technique, when the error minimized between the focal position and template obtained before, the focused image is obtained. The limitation of this method is that a new template is needed to feed the proposed technique if the micropipette is changed. Additionally, the matching process of the injection pipette contains all possible locations in the sourced image, which increases the computational cost of the technique. Microfingers are microgrippers which are made from a hollow glass tube and used for gripping and handling biological cells [16], [17]. The depth of field for the tip of the micro-fingers can be searched by using color information along with template matching techniques as the shape of the finger is fixed during the injection task [18]. Color information helps to find the correct direction of the focal plane. However, any method for positioning the micro-objects using template matching technique is not an effective way to track the micro-objects without a clear morphology [19]. On the other hand, any method using the template matching technique is computationally expensive [20].

The inner space of the holding pipette can also be utilized for focal plane estimation. When the inner space of the holding pipette has the highest width value, then it is claimed that the image is the focal plane [21]. Due to the large set of pre-recorded image collection before applying the image processing algorithm, utilization of the width of the holding pipette is not practical. This is due to changes in image processing algorithm parameters, and the image collection task would need to be repeated.

Contrast measurement greatly affects the accuracy of the focusing procedure but the efficiency of the FMA depends on the peak search algorithm used. A variety of search strategies have been proposed in the literature to drive the focus motor in the desired position. Global search is the most widely-known method. In this method, all focal positions are scanned and the peak point is detected. Therefore, there is no possibility of detecting a wrong focal position. Conversely, this method is not practical when the high focus range is needed for a specific application and it requires high computation time. Fibonacci and particle swarm optimization with Gaussian jump are studied in the literature in which suitability of the search algorithm depends on the shape of the focus curve [22], [23]. Since the result of the developed auto-alignment algorithm produces unimodal curve after evaluation of the 12 different focus measure algorithms, a Fibonacci search algorithm has been found to be an appropriate search method and is implemented into the developed algorithm for auto-alignment of the injection pipette task. This method is further improved using curve fitting to eliminate local optimum disturbance [24]. Implementation of a Fibonacci search algorithm requires a motorized stage to be driven with a high resolution for the precise alignment of the pipettes. Suitable focus algorithms and searching methods are two essential parameters for a successful auto-alignment of the injection pipette process.

This study aims to propose a technique for auto-aligning the injection and holding micropipettes for the oocyte injection task. The details of the auto-alignment technique and experimental validations are presented.

II. SYSTEM DESIGN

A. SYSTEM CONFIGURATION

Fig. 1 shows the system setup which consists of a Bestscope 2700 inverted microscope, a microscopy camera (BASLER Camera acA1300-200um - Python1300), a holding micropipette with a 120 μm outer diameter (Smiths Medical-Wallace WHP-120B-30, USA) and a 5.5-μm spiked tip ICSI injection micropipette (Smiths Medical-Wallace WIC-55H-30, USA). Images are captured through a 40x objective lens in maximum lighting conditions. Captured images are processed by an Intel®Core^{TM}i5-6500 CPU @3.2 GHz (4 CPUs) host computer. The 8MT167 3-DOF motorized stage from Standa is employed to control the position of the holding and injection pipette with the resolution of less than 1 μm. The produced vibration during the alignment procedure is damped using an anti-vibrational table.

B. METHOD OVERVIEW

During the auto-alignment operation, the pipettes are initially detected using the visual detection algorithm and then are manipulated automatically using the information received from the focus curve and focus algorithm. A focus curve demonstrates the focusing position of the pipette based on a calculated focus value obtained from focusing algorithms. The behavior of the focus curve plays a crucial role in the alignment of the injection and holding pipette. Ideally, the focus curves obtained from focus algorithms should be unimodal and sharp at the top and long-tailed. However, some

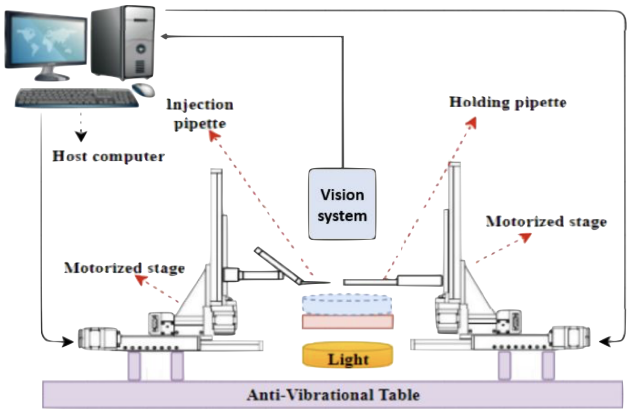

FIGURE 1. System setup for the auto-alignment procedure.

focus algorithms may present various local maxima or the same focus value at different focal positions. This causes an error in the accurate measurement of the focus point. Therefore, evaluation of the focus algorithms is essential to find a suitable algorithm to implement for auto-alignment of the pipettes. In this study, different focusing functions were compared quantitatively, and focus curves were normalized to obtain the most accurate algorithm for each injection and holding pipette. The Fibonacci search algorithm was then implemented to drive the injection and holding pipette in Z-axis independently to position them in focal plane.

In the following section, 12 different focus algorithms are described briefly which are used to obtain the optimum focus curve.

C. AUTOFOCUS FUNCTIONS

A variety of focus algorithms have been proposed in the literature to find the optimal algorithm for a specific application. Ideal focus curve is defined as having the sharpest image at the maximum value of the focus curve. This value decreases once the images demonstrate further distance positions from the focal plane. To obtain the initial position of the pipettes, an automated stage moved the pipettes in Z-axis until the micropipettes become partially visible in the field of view. The focalization procedure of the pipettes starts after immediate detection of the pipette. To measure the focus values by implementing each algorithm, the stage moved in an increment of 2 and 10 μm for the injection and holding pipette respectively and scanned the pipettes. The focus curves are then obtained based on the algorithm results. In this study, twelve different focus algorithms were examined, evaluated and compared for each pipette separately to find the optimum algorithm demonstrating a good distribution of the values in a curve and to conclude a single focal plane. The measured values obtained from the algorithms are correlated to the position of the stage. Consequently, the focal level was calculated based on home position and the differences between each incremental movement of the stage which was linked to the focus curve.

This is the first report on the extensive evaluation of the Focus Measure Functions (FMA) in the field of oocyte manipulation and sperm injection. The FMA used in this paper can be classified as derivative-based, statistical-based and histogram-based algorithms.

Derivative-Based Algorithms:

1. Thresholded gradient: The sharpness of an image is proportional to the high frequency of an image and high pass filters are widely used to detect the high frequency of the portions of an image [25]. The thresholded gradient algorithm computes the first difference of the pixel intensities and then accumulates if it reaches above the specified threshold. Therefore, this algorithm reveals a larger gradient in the image. The focalization value is given in equation (1) [26].

$$F_{th\_grad} = \sum_{M}\sum_{N} |g(i,j+1) - g(i,j)| \tag{1}$$

$$\text{While } |g(i,j+1) - g(i,j)| \geq v \tag{2}$$

where g (i, j) represents the gray level intensity of pixel (i, j), and v the gradient threshold. In this algorithm, M x N image is used where M and N present the height and width of an image respectively in pixels.

2. Modified Laplacian: A modified Laplacian as a focus measure function is computed at a point (i, j) in a window around (i, j), which is greater than a threshold value [27]. Equation (3) demonstrates how this method uses the discrete approximation of the Laplacian to compute the second derivatives in the horizontal and vertical direction of an image.

$$F(i,j) = \sum_{x=i-N}^{i+N}\sum_{y=j-N}^{j+N} ML(x,y) \; for \; ML(x,y) \geq T_1 \tag{3}$$

where N represents the window size used to compute the focus measure function. N is taken normally 1 or 2 as the modified Laplacian method uses very small window size such as 3-by-3 or 5-by-5.

3. Tenengrad Gradient: In this algorithm, convoluted images are used along with Sobel operators to compute the first difference as in equation (4) [12].

$$F_{tenengrad} = \sum_{height}\sum_{width} (S_x(x,y)^2 + S_y(x,y)^2) \tag{4}$$

where $S_x(x, y)$ and $S_y(x, y)$ are the convoluted images with Sobel operators.

4. Brenner Gradient: The Brenner gradient algorithm calculates the square difference of each pixel between its two neighbors on the image used and then sums them together using the equation (5) [11].

$$F_{brenner} = \sum_{x,y} i(x+1,y) - i(x-1,y))^2 \tag{5}$$

with |i(x+1), y) – i(x-1), y)| > a, where i (x, y) is the intensity at pixel (x, y), a is the threshold of the intensity difference.

5. Energy of Gradient: Gradient energy of a single pixel demonstrates a certain difference between focus and unfocused image. The energy of gradient focus measure function is computed as below equations (6), (7) and (8) [13], [28].

$$F_{energy_{grad}} = \sum_{x} \sum_{y} (g_x^2 + g_y^2) \tag{6}$$

where

$$g_x(x, y) = g_i(x + 1, y) - g_i(x, y) \tag{7}$$

And

$$g_y(x, y) = g_i(x, y + 1) - g_i(x, y) \tag{8}$$

6. Spatial Frequency: This is a modified version of the Energy of the gradient algorithm. In this algorithm, M x N image is used where M and N present number of rows and columns respectively, along with gray value F (j, k) at position (j, k) [29]. The row and column frequencies are given in equation (9) and (10).

$$R_F = \sqrt{\frac{1}{MN} \sum_{J=0}^{M-1} \sum_{k=1}^{N-1} [F(j, k) - F(j, k-1)]^2} \tag{9}$$

and

$$C_F = \sqrt{\frac{1}{MN} \sum_{k=0}^{N-1} \sum_{J=1}^{M-1} [F(j, k) - F(j-1, k)]^2} \tag{10}$$

The total frequency is calculated as in equation (11).

$$Spatial\ frequency = \sqrt{(R_F)^2 + (C_F)^2} \tag{11}$$

Statistical Algorithms:

7. Gray Level Variance: While sharp images show high gray level variance, the images associated with blurring have low gray level variance. The simple standard definition of image variance is adopted into the equation given below. The equation (12) is used as a focus measure function using gray level variance [12].

$$\sigma^2 = \frac{1}{N^2} \sum_{x=1}^{N} \sum_{y=1}^{N} [I(x, y) - \mu]^2 \tag{12}$$

where μ is the mean of the gray level variance. The aim here is to maximize the σ^2 value since increases in σ^2 value will let us obtain higher gray level variance, therefore sharper image.

8. Tenengrad Variance: Another focus measurement alternative to get the gradient information is to calculate the gradient magnitude. In this direction, Tenengrad focus measure is calculated by the following equation (13) [30].

$$F_{tenengrad_{variance}} = \sum_{m}^{M} \sum_{n}^{N} [S(m, n) - S']^2 \ and\ for\ S(m, n) > T \tag{13}$$

where T is the threshold, M and N are the height and width of an image, respectively. S' is the mean of magnitudes which is given by equation (14).

$$S' = \frac{1}{NM} \sum_{m}^{M} \sum_{n}^{N} S(m, n) \tag{14}$$

9. Variance of Laplacian: This method calculates the variance of the absolute values which provides a new focus measurement [30]. The equation (15) is demonstrated as:

$$F_{laplacian\_variance} = \sum_{m}^{M} \sum_{n}^{N} [|L(m, n)| - L']^2 \tag{15}$$

where L (m, n) is the convolution of the input image I (m, n) with the Laplacian operator L which can be approximated using the following mask:

$$L = \frac{1}{6} \begin{pmatrix} 0 & -1 & 0 \\ -1 & 4 & -1 \\ 0 & -1 & 0 \end{pmatrix} \tag{16}$$

and L' is the mean of absolute values given by

$$L' = \frac{1}{NM} \sum_{m}^{M} \sum_{n}^{N} |L(m, n)| \tag{17}$$

10. Vollath's Correlation: This focus measure function is based on autocorrelation function and is computed as in equation (18) [26].

$$F_{vollath's} = \left(\sum_{i=1}^{M-1} \sum_{j=1}^{N} g(i, j) .g(i + 1, j)\right) - \left(\sum_{i=1}^{M-2} \sum_{j=1}^{N} g(i, j) .g(i + 2, j)\right) \tag{18}$$

The advantage of this method is that it does not depend on a threshold while some of the focus function does.

11. Image Curvature: Image curvature can be utilized as a focus measure since the curvature is higher in sharp images than blurred images [31]. In this method, the gray values are considered as a 3D surface (x, y, t(x, y). First of all, the quadratic equation $f(x, y) = kx + ly + mx^2 + ny^2$ is used to approximate the surface. After that the least square approximation technique is used with t_0 *and* t_2 to calculate the coefficients (k, l, m, n).

$$t_0 = \begin{pmatrix} -1 & 0 & 1 \\ -1 & 0 & 1 \\ -1 & 0 & 1 \end{pmatrix} \ and\ t_2 = \begin{pmatrix} 1 & 0 & 1 \\ 1 & 0 & 1 \\ 1 & 0 & 1 \end{pmatrix} \tag{19}$$

Finally, the coefficients are combined and focus measure is obtained as in equation (20).

$$F_{curvature} = |k| + |l| + |m| + |n| \tag{20}$$

Histogram-Based Algorithms:

12. Histogram Entropy: Let P (I) represents the frequency of the gray level I. The histogram entropy is defined by equation (21) [12].

$$E = -\sum_{I} P(I) \ln [P(I)] \quad P(I) \neq 0 \tag{21}$$

'E' reaches its maximum value when all P (I) are equal, and minimum values when P (I) = 0 for all but one value of I. In this case, sharper images have smaller entropy than blurred images. Therefore, minimizing the value of E will give the sharper image. This algorithm has also been evaluated and compared in previous researches [26], [32].

III. AUTO-ALIGNMENT OF THE INJECTION AND HOLDING PIPETTE

Focalization provides key information in Z-axis for automatic leveling of the pipettes to the focus. In the following section, the focalization of the injection and holding pipette and their alignment with each other will be given.

A. AUTOFOCUSING OF THE INJECTION AND HOLDING PIPETTE

For focalization of the injection pipette, a set of 18 images was captured for the injection pipette by scanning the movement of the pipette among Z-axis in a range between 0 to 34 micrometers using 2 micrometers increments. The initial position is obtained as the most blurred image captured below the focal plane, and the final destination position represents the most blurred image obtained above the focal plane. This means that any distance above or below this level brings the pipettes fully out of focus.

A similar image acquisition process is also conducted for the holding pipette focalization. Similarly at the beginning of the operation, a set of 18 images was captured in a range between 0 to 170 micrometers by scanning with a 10 micrometers increment. Under the assumption of achieving 100% accurate focalization for the injection pipette, it should be possible to insert the injection pipette into the holding pipette without causing any bending when it goes through the holding pipette as long as the holding pipette is in alignment as well. The inner diameter of the holding and injection pipette is 30μ and 5.5 μ, respectively. In this case, the tolerance of the developed auto-alignment process is 12.25 μ.

Digital images are generally exposed by noise. The level of noise is propagated during the image acquisition and transmission process. Therefore, pre-processing is often required to prevent the negative influence of the noise on developed algorithm performance [33]. A Gaussian filter as a part of pre-processing is implemented to reduce the noises on the captured image for the injection and holding pipette. Subsequently, the adaptive image threshold using first order statistics is used to obtain the binary image of the injection pipette. This process is called thresholding. Employing binary image procedure is not practical for the holding pipette since it has an inner reflection under the microscope particularly when the higher magnification is utilized. In this case, the active contour method is implemented on the holding pipette along with a defined focus window where all focus algorithms are applied [34].

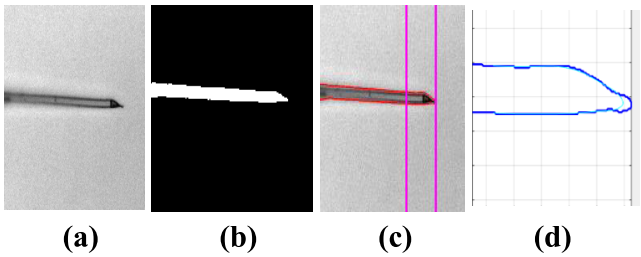

FIGURE 2. Region of Interest extraction. (a) Original injection pipette image. (b) Final binary image. (c) Image with a boundary at the ratio of 1:4 divided by lines. (d) Extraction of region of interest.

The boundaries of the injection pipette are detected by using the obtained binary image. However, the level of smoothness of the boundary demonstrates irregular data points at some fragment of the boundaries for both injection and holding pipettes. This can be seen in Fig. 2 and 3. Hence, Kernel smoother, which is a statistical technique widely used in engineering, is utilized on the boundary of the injection and holding pipettes to obtain for better data visualization. This is because the Kernel smoother represents the set of irregular data points on the boundary of pipettes as a smooth line. The extracted boundary is taken as a reference to plot two different lines which divide the boundary of the injection pipette at the ratio of 1:4 of the extracted boundary from the tip of the injection pipette. The mask is created within the region of interest where all focus algorithms are applied. Fig. 2 represents the procedure of the pipette marginal detection and indicates the region of the interest extraction procedure for the injection pipette.

The mask is created in the focus window after implementing the active contour method on the holding pipette with a defined focused window. The region of interest for the holding pipette is extracted at the ratio of 3:4 from the tip of the holding pipette. The ratio selection to extract the region of interest for both injection and holding pipettes was selected to provide sufficient information to the FMA methods for their analysis. The implemented image processing technique is sufficient for holding pipette focalization due to its size. The obtained data variations on the recorded images using lower than 10 μm increment are not significantly different. Consequently, 10 μm is selected to be the optimum increment and also this increment is within the tolerance. Fig. 3 represents the region of interest extraction for analysis of the focus algorithms in-focus plane.

B. CURVE FITTING AND FIBONACCI SEARCH ALGORITHM

Curve fitting is the process of building a curve that has the best fit to the data points. In order to minimize the number of images captured to estimate the focal position of the injection and holding pipette, autofocusing is carried out by the mathematical function that accurately mimics the focus curve. It is essential to have sufficient data points near the focal

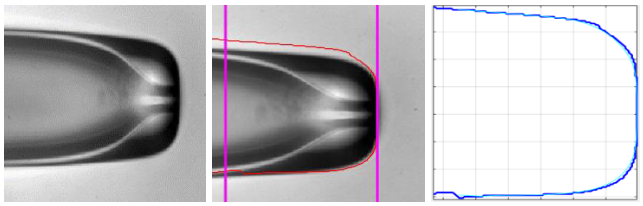

FIGURE 3. Region of Interest extraction. (a) Original holding pipette Image. (b) Holding pipette contour detection and its division by lines at the ratio of 3:4. (c) Extraction of the region of interest.

plane with the purpose of having accurate auto-alignment of the pipettes. Global maxima and minima are defined as the largest and the smallest value of the mathematical function obtained from the curve fitting, respectively. The obtained focal position could be a global maximum or minimum depending on the FMA used. However, in this study, the focus curve is inverted to global maxima if the FMA produces a global minimum focal point. Here, the second-order Gaussian fit is implemented to the focus curves to obtain the focus function of the focus curve [27].

In order to search the focal plane of the injection and holding pipette precisely, a Fibonacci search algorithm was employed to find the global maximum point of the focus curve function. The search interval was introduced to the Fibonacci search algorithm; it successively narrows the search interval until a satisfactory approximation for focus is achieved [22]. A Fibonacci search algorithm was an appropriate algorithm as long as the curve shows the unimodal property. Under the unimodality assumption of the focus curves for holding and injection pipettes, it has been proven that the Fibonacci search algorithm is the optimal algorithm [35].

C. ALIGNMENT OF THE INJECTION PIPETTE TO THE HOLDING PIPETTE

Before the alignment operation started, the pipettes were randomly inserted into the pipette holders. This caused no exact identification of the pipette tips initial position. Each position after initial detection had a corresponding focus value on the graph. Consequently, the proposed algorithm calculated the differences between the focal position and the current position values. These differences provide sufficient information to the developed algorithm to understand whether the tip of the pipettes is below or above the focal plane. Then the system determined the accurate corresponding positions and their differences. Once the pipettes were located to the focal plane, the coordinate of the pipette tips in X and Y-axis were calculated. The pixel coordinate of the tip of the pipettes was obtained by a set of image processing algorithms. This was achieved by obtaining the binary image of the pipettes using adaptive image threshold and their blob detection once they were in focus. Blob detection is a computer vision method that detects the regions in the image by distinguishing them in terms of pixel mean intensity, perimeter and the area of the blob. Here the pipettes were distinguished from each other in terms of their blob pixel area. After detection of the pipettes in binary form, on the far right of the pixel of the injection pipette and on the far left pixel of the holding pipette, they were both detected and reported. Obtaining the binary form of the holding pipette is only practical when it is in focus. Then, the pipettes are travelling only in the XY plane to grasp the oocyte and bring it to the predefined position and then conduct the injection when all are in focus.

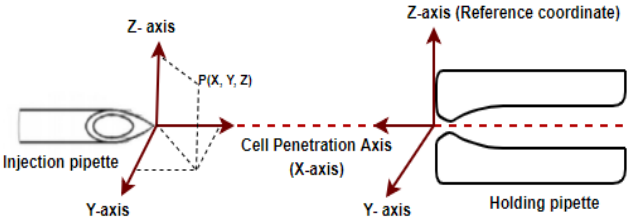

FIGURE 4. Schematic 3D view of the injection and holding pipette.

The schematic 3D view of the injection and holding pipette is given in Fig. 4. As demonstrated, the leveling of the pipettes were conducted in Z-axis. However, the final grasping and injection are conducted in XY plane.

IV. RESULTS AND DISCUSSION

This section presents and discusses the obtained results from auto-focusing algorithms for the auto- focalization procedure of the pipettes for the oocyte injection task. In this section, the results for the automatic alignment of both the holding and injection pipettes are presented separately. Then the operational confirmation will be experimentally demonstrated by inserting the injection pipette into the holding pipette. This fully illustrates that both pipettes are in absolute focus and within the same XY plane.

A. FOCUS MEASUREMENT ALGORITHM RESULTS

Fig. 5 shows the results of focus curves obtained from twelve focusing algorithms for auto-focusing of the injection pipette. In each graph, the normalized focus measure is demonstrated versus pipette position reported by the motorized stage.

Based on the results in Fig. 5, Energy of gradient, Vollath correlation, Gray level variance, and Brenner gradient methods produced reasonable focus curves as the rest of the methods produced false local maxima. Additionally, producing a unimodal curve is essential to enable the Fibonacci search algorithm to find the peak point of the curve accurately.

Focalization of the holding pipette is also essential for the auto-alignment task for an oocyte injection procedure. Fig. 6 presents the results of the focus curves obtained from focusing algorithms for auto-focusing of the holding pipette. All focus values are normalized and plotted versus stage position.

From the data in Fig. 6, it is apparent that very few FMA were able to produce a sensible focus curve. This is due to the light reflection of the inner space of the holding pipette where there was not any such noise as in the injection pipette.

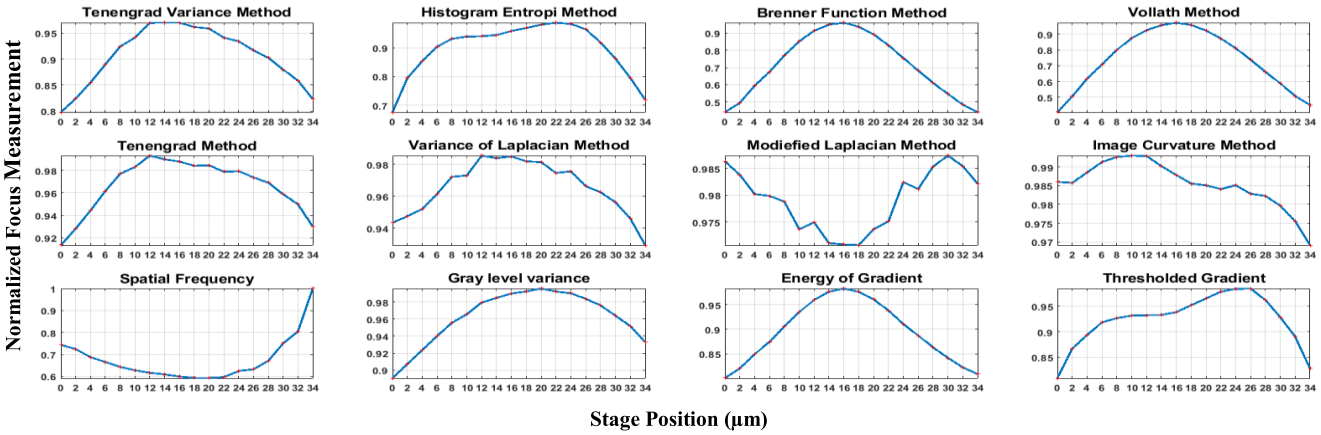

FIGURE 5. Auto-focusing of the Injection pipette based on different focus measurement algorithm.

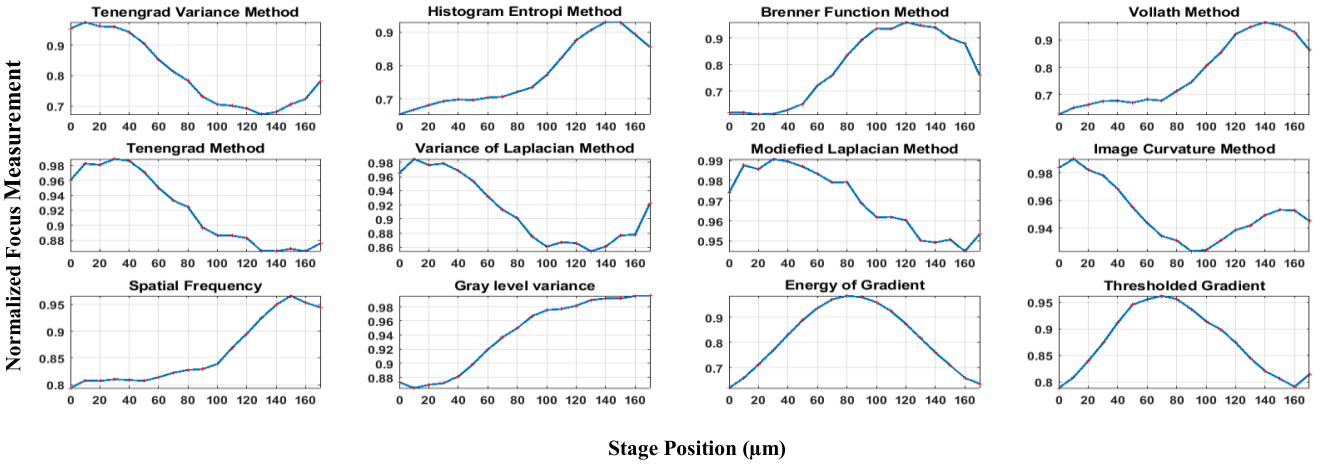

FIGURE 6. Auto-focusing of the Holding pipette based on different focus measurement algorithms.

Only the Energy of gradient method was able to produce a gradable focus curve.

The performance of the focus curves is evaluated based on focusing accuracy, range, number of false maxima and the width of the curve [36]. Accuracy is measured from the differences between the determined best focus positions manually and the peak position of the curve obtained from the focus algorithm. A smaller accuracy value gives a more accurate focus position of the injection and holding pipettes. Range criteria measure the distance between two adjacent local minima of the peak points in the focus curve. The larger range of focus curve will help searching algorithm to find the global peak without being trapped between two minima points during the search. A number of false maxima describe any other peak points of the curve apart from the global maximum. The width of the focus curve illustrates the sharpness of the peak as the sharper curve at the peak point has given a more accurate focus position to drive injection and holding pipette. In this paper, 50% of the height of the curve is evaluated as the width of the curve.

Based on the results obtained from Fig. 5 and 6, focus evaluation parameters are demonstrated in Table 1. The desired value for accuracy, number of false maxima and the width of the curve at %50 is 0, while the desired value for range criteria is 1. For the evaluation of the FMA, the difference between the desired criterion's value and the value of the focus curve for each criterion is taken as a coordinate. Maximum range criteria are subtracted from the range value of each FMA for calculation of the overall performance. Hence, the desired distance coordinate of the focus curve is [0 0 0 0] since 4 different criteria are used in this study. The overall score is calculated as a Euclidean distance for the focus curve obtained. If the given criteria are not applicable to the focus curve obtained, maximum focus criterion value is taken into account for Euclidean distance calculation. All values for each criterion are normalized and given within a range of between 0 and 1 so that each evaluation parameter maintains the equal weight for the overall performance comparison. The lower overall score presents the better performance of the focusing algorithm which is essential to have higher accuracy Z-axis focalization of the micropipettes.

TABLE 1. Injection and holding pipette's focus curves overall evaluation.

FMA	Accuracy		Range		Number of false maxima		The width of the curve at %50	
	Injection pipette	Holding pipette	Injection pipette	Holding pipette	Injection pipette	Holding pipette	Injection pipette	Holding pipette
Thresholded gradient	0.55	0.11	1	0.94	0.4	0.2	1	1
Energy of gradient	0	0	1	1	0	0	0.857	0
Gray-level variance	0.22	1	1	0.058	0	0.6	1	1
Modified Laplacian	0.77	0.55	0.058	0.058	0.8	1	1	1
Image Curvature	0.22	0.77	1	0.058	0.8	0.6	1	1
Tenengrad	0.22	0.22	1	0.176	0.6	0.6	0.857	1
Tenengrad variance	0.22	0.77	1	0.058	1	0.6	0.821	1
Variance of Laplacian	0.22	0.77	1	0.0176	0.8	0.8	0.785	1
Vollath's correlation	0	0.66	1	0.058	0	0.4	0.785	1
Brenner gradient	0	0.66	1	0.176	0	0.8	0.714	1
Spatial frequency	1	0.77	0.058	0.058	1	0.4	1	1
Histogram entropy	0.33	0.66	1	0.058	0.4	0.4	0.928	1

As it is pointed out in Table 1 for the evaluation of the injection pipette, Brenner gradient, Vollath correlation and Energy of gradient demonstrated 100% accuracy while Gray-level variance illustrated 88% accuracy. The tolerance assumption for holding pipette alignment was conditioned with 100% accuracy of the injection pipette. Hence, 88% accuracy has not been considered. Among the methods giving 100% accuracy, the only difference was obtained in the width of their curves at 50%. This is a significant parameter that needs to be considered for FMA evaluations. This is because the lower width at 50% of the curve not only demonstrates how sharp the peak point of the curve is but also illustrates a higher focus measurement range. This is an essential feature to be obtained for auto-alignment of the pipettes. A distinguishable focus measurement value between different focus levels at a small distance to each other helps the auto-alignment procedure remarkably, particularly around the focal plane. Brenner gradient provided the smallest width of the curve at 50% among all focus methods while providing 100% accuracy, full range with no false maxima as shown in Table 1. Hence, Brenner gradient demonstrated better performance than Vollath correlation and Energy of gradient method based on the calculation of the Euclidian method.

Fig. 6 makes it evident that most of the FMA were exposed with a high noise for holding pipette focalization. This is due to the inner reflection of the holding pipette as stated previously. The 11 out of 12 FMA algorithms were failed with the exception of Energy of gradient method. The result of the thresholded gradient method also produced a gradable curve. However, the focus measurement value at the last frame was always higher than the previous frame. This causes a disturbance in the Fibonacci search algorithm to find the peak point of the curve. The correct detection of the peak point of

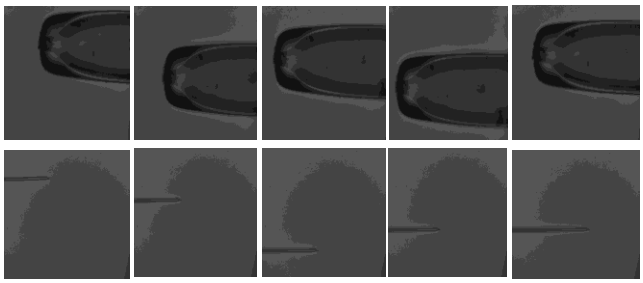

FIGURE 7. Auto-focusing of the pipettes at random positions in XYZ.

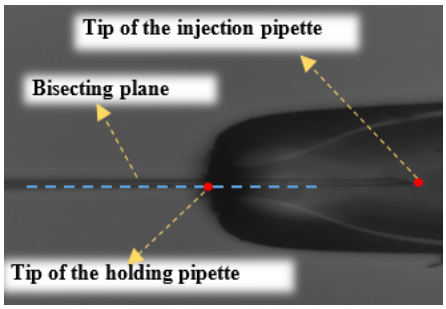

FIGURE 8. Auto-alignment of the pipettes for oocyte injection.

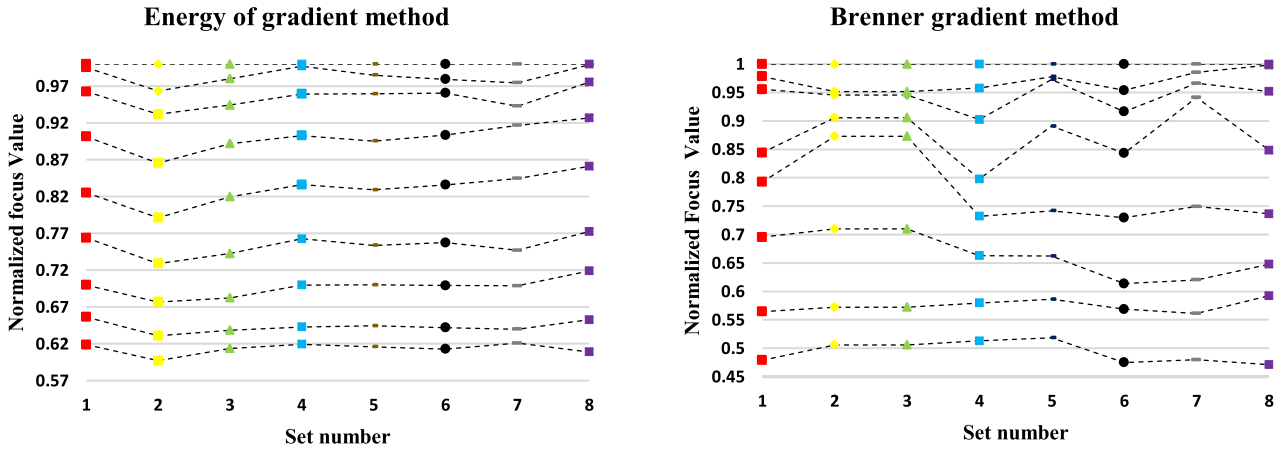

FIGURE 9. Focus value variations of the injection and holding pipette at different positions.

TABLE 2. computational time analysis for auto-alignment of the pipettes in overall.

FMA	Averaged Computation Time per Frame (s)	Standard Deviation
Brenner Gradient	1.159	0.0106
Energy of Gradient	1.717	0.0252

the curve of the Energy gradient method was 100%. This is in a decent agreement with the tolerance of the holding pipette alignment. Overall, the Energy of gradient algorithm was found to be the most suitable for holding pipette focalizations for the purpose of the auto-alignment procedure.

The Energy of gradient and Brenner gradient methods are both derivative-based FMA. This type of algorithm tends to be affected by noise while providing better accuracy in comparison to statistical algorithms [36]. With the aid of comprehensive evaluation of the FMA, decent accuracy for focalization of the pipettes was achieved whilst selected algorithms were not affected by any type of disturbance during their operation. The feature of the insensitivity of the noise for the developed auto-alignment process while providing high accuracy will be well proved in the following section.

Computational time is also an essential parameter to be considered to increase the productivity of the developed algorithm. Computational time is highly dependent on the quality of the image and the number of pixels processed. For the analysis of the computational time, 8 sets of image collection for holding and injection pipette focalization were captured separately at random positions in the XYZ plane. Each set consists of 18 images for both pipettes and was run 15 times and then the averaged computation time was recorded. Recorded computation times include the entire computation to run the algorithm. Subsequently, the average computation time of 8 sets was recorded along with its standard deviation. Table 2 illustrates the average computational time per frame for performing the auto-alignment of the pipettes.

The alignment procedure calculation was conducted only once and the operational distance was calculated based on that particular frame which does not require additional image acquisition for any rest of the images within each trial.

B. VALIDATION TEST RESULTS FOR ICSI INSERTION TO THE HOLDING PIPETTE

In this section, the effectiveness of the developed image-based auto-alignment of the Injection pipette is shown experimentally. It is motivated to conduct the insertion of the injection pipette within the holding pipette to illustrate the accuracy of leveling of the pipettes. This is a reasonable test to visually validate the leveling of micropipettes. This proved the operational accuracy of the algorithm in focusing the pipettes. Each pipette is randomly positioned at different levels in XYZ and programmed to be inserted. A total of 100 experiments have been conducted to prove this hypothesis. All of the insertion was conducted without any failure. The results approved the high reliability of the algorithm in different stages of pipette detection, operation calculation, and manipulation. Fig. 7 and 8 demonstrate an example of the different positioning of pipettes and insertion experiment.

The experimental results illustrate that the developed image-processing algorithm can perform the auto-alignment procedure successfully regardless of the pipettes' positions. The developed method can perform an auto-alignment even if the position of injection and holding pipette images are not within the recognition ranges.

In order to assess the trade-off between the sensitivity of the focalization of the pipettes to the noises and also their reliability at the same focal levels at different positions on the image plane, another set of experiments was carried out. In this experiment, the pipettes were randomly positioned at 8 different locations. The number of focus levels for each set is limited where the pipettes are in focus. For each position, 18 images were captured above and below the focal point with a 10 and 2-micrometers increment to each other for holding

and injection pipettes, respectively. Fig. 9 demonstrates the normalized focus value versus the set number.

In Fig. 9, each color represents one set of experiments and each set is evaluated within itself. Hence, there is no continuity between sets in terms of their data points. No intersections between the indicated dashed lines were observed for the pipettes as illustrated in Fig. 9, which clearly demonstrate the reliability of the algorithm for an oocyte injection operation. This also demonstrates that the values are only dependent on the image set and are not a general measure for each level.

This study demonstrates the first reporting of auto-alignment of the pipettes used in ICSI with a combined computational time for pipette detection and alignment of 3s. This is in contrast to a much larger corresponding value of 14s reported in a similar study conducted for holding pipette [21], hence offering a considerable reduction in computational cost. Additionally, the results indicate 100% accuracy in both detection and alignment, enhanced reliability, and insensitivity to noise at different positions in the image plane.

V. CONCLUSION

This paper offers a technique to automatically align the injection and holding pipette under microscopy imaging for ICSI operation. A ranking methodology was implemented on twelve different focus measure algorithms to determine the most appropriate focus algorithm in ICSI operation. The Fibonacci search algorithm has been implemented into the developed technique to drive the z-axis of the motorized stage to the focus position. It has been demonstrated that the Brenner gradient and Energy of gradient algorithms have superior performance for the injection and holding pipette focalization respectively. The results show that the auto-alignment tasks were achieved with high accuracy, reliability and demonstrated insensitivity to noises at different positions in the image plane.

ACKNOWLEDGMENT

The authors would like to thank UK Medical Research Council (MRC) for their support of aspects of this work. The authors also wish to thank Basler AG for their contribution in the vision development part of this work.

REFERENCES

[1] G. Palermo, H. Joris, P. Devroey, and A. C. Steirteghem, "Pregnancies after intracytoplasmic injection of single spermatozoon into an oocyte," *Lancet*, vol. 340, nos. 88–10, pp. 17–18, Jul. 1992.

[2] H. B. Huang, D. Sun, J. K. Mills, and S. H. Cheng, "Robotic cell injection system with position and force control: Toward automatic batch biomanipulation," *IEEE Trans. Robot.*, vol. 25, no. 3, pp. 727–737, Jun. 2009.

[3] Y. H. Anis, M. R. Holl, and D. R. Meldrum, "Automated selection and placement of single cells using vision-based feedback control," *IEEE Trans. Autom. Sci. Eng.*, vol. 7, no. 3, pp. 598–606, Jul. 2010.

[4] R. Kumar, A. Kapoor, and R. H. Taylor, "Preliminary experiments in robot/human cooperative microinjection," in *Proc. IEEE/RSJ Int. Conf. Intell. Robots Syst.*, Oct. 2003, pp. 3186–3191.

[5] Q. Zhao, M. Sun, M. Cui, J. Yu, Y. Qin, and X. Zhao, "Robotic cell rotation based on the minimum rotation force," *IEEE Trans. Autom. Sci. Eng.*, vol. 12, no. 4, pp. 1504–1515, Oct. 2015.

[6] Z. Nan and Q. Xu, "Multiple-cell recognition and path planning for robotic microinjection system," in *Proc. 36th Chin. Control Conf. (CCC)*, Jul. 2017, pp. 6691–6696.

[7] Z. Lu, X. Zhang, C. Leung, N. Esfandiari, R. F. Casper, and Y. Sun, "Robotic ICSI (intracytoplasmic sperm injection)," *IEEE Trans. Biomed. Eng.*, vol. 58, no. 7, pp. 2102–2108, Jul. 2011.

[8] R. Redondo, G. Cristóbal, G. B. Garcia, O. Deniz, J. Salido, M. D. M. Fernandez, J. Vidal, J. C. Valdiviezo, R. Nava, B. Escalante-Ramírez, and M. Garcia-Rojo, "Autofocus evaluation for brightfield microscopy pathology," *J. Biomed. Opt.*, vol. 17, no. 3, 2012, Art. no. 36008.

[9] N. Kehtarnavaz and H.-J. Oh, "Development and real-time implementation of a rule-based auto-focus algorithm," *Real-Time Imag.*, vol. 9, no. 3, pp. 197–203, Jun. 2003.

[10] S. K. Nayar, M. Watanabe, and M. Noguchi, "Real-time focus range sensor," *IEEE Trans. Pattern Anal. Mach. Intell.*, vol. 18, no. 12, pp. 1186–1198, Dec. 1996.

[11] J. F. Brenner, B. S. Dew, J. B. Horton, T. King, P. W. Neurath, and W. D. Selles, "An automated microscope for cytologic research a preliminary evaluation," *J. Histochem. Cytochem.*, vol. 24, no. 1, pp. 100–111, 1976.

[12] E. Krotkov, "Focusing," *Int. J. Comput. Vis.*, vol. 1, no. 3, pp. 223–237, Oct. 1988.

[13] M. Subbarao, T.-S. Choi, and A. Nikzad, "Focusing techniques," *Opt. Eng.*, vol. 32, no. 11, pp. 2824–2837, 1993.

[14] Y. Qiu, "NIH public access," *Anal. Cell Pathol.*, vol. 36, pp. 37–44, 2013.

[15] Y. Sun and B. J. Nelson, "Biological cell injection using an autonomous microrobotic system," *Int. J. Robot. Res.*, vol. 21, nos. 10–11, pp. 861–868, 2002.

[16] T. Tanikawa, T. Arai, and N. Koyachi, "Development of small-sized 3 DOF finger module in micro hand for micro manipulation," in *Proc. IEEE/RSJ Int. Conf. Intell. Robots Syst., Hum. Environ. Friendly Robots High Intell. Emotional Quotients*, Oct. 1999, pp. 876–881.

[17] C.-N. Nguyen, K. Ohara, E. Avci, T. Takubo, Y. Mae, and T. Arai, "Automated micromanipulation for a microhand with all-in-focus imaging system," in *Proc. IEEE/RSJ Int. Conf. Intell. Robots Syst.*, Sep. 2011, pp. 427–432.

[18] A. Suzuki, Y. Mae, T. Tanikawa, T. Arai, and K. Inoue, "Automated micro handling," in *Proc. IEEE Int. Symp. Comput. Intell. Robot. Automat., Comput. Intell. Robot. Automat. New Millennium*, Jul. 2003, pp. 348–353.

[19] J. Liu, Z. Gong, K. Tang, Z. Lu, C. Ru, J. Luo, S. Xie, and Y. Sun, "Locating end-effector tips in robotic micromanipulation," *IEEE Trans. Robot.*, vol. 30, no. 1, pp. 125–130, Feb. 2014.

[20] Y. Zhang, K. K. Tan, and S. Huang, "Vision-servo system for automated cell injection," *IEEE Trans. Ind. Electron.*, vol. 56, no. 1, pp. 231–238, Jan. 2009.

[21] Z. Wang, C. Feng, W. T. Ang, S. Y. M. Tan, and W. T. Latt, "Autofocusing and polar body detection in automated cell manipulation," *IEEE Trans. Biomed. Eng.*, vol. 64, no. 5, pp. 1099–1105, May 2017.

[22] E. P. Krotkov, *Active Computer Vision by Cooperative Focus and Stereo*. New York: NY, USA: Springer, 2012.

[23] I. M. Bahadur and J. K. Mills, "Robust autofocusing in microscopy using particle swarm optimization," in *Proc. IEEE Int. Conf. Mechatron. Automat.*, Aug. 2013, pp. 213–218.

[24] Y. Xiong and S. A. Shafer, "Depth from focusing and defocusing," in *Proc. IEEE Conf. Comput. Vis. Pattern Recognit.*, Jun. 1993, pp. 68–73.

[25] L. C. Chiu and C. S. Fuh, "An efficient auto focus method for digital still camera based on focus value curve prediction model," *J. Inf. Sci. Eng.*, vol. 26, no. 4, pp. 1261–1272, Jul. 2010.

[26] A. Santos, C. Ortiz-solórzano, J. J. Vaquero, J. M. Peña, N. Malpica, and F. D. Pozo, "Evaluation of autofocus functions in molecular cytogenetic analysis," *J. Microsc.*, vol. 188, pp. 264–272, Dec. 1997.

[27] S. K. Navar, "Shape from focus," Carnegie Mellon Univ., Tech. Rep., 1989.

[28] W. Huang and Z. Jing, "Evaluation of focus measures in multi-focus image fusion," *Pattern Recognit. Lett.*, vol. 28, no. 4, pp. 493–500, 2007.

[29] A. M. Eskicioglu and P. S. Fisher, "Image quality measures and their performance," *IEEE Trans. Commun.*, vol. 43, no. 12, pp. 2959–2965, Dec. 1995.

[30] J. L. Pech-Pacheco, G. Cristobal, J. Chamorro-Martinez, and J. Fernandez-Valdivia, "Diatom autofocusing in brightfield microscopy: A comparative study," in *Proc. 15th Int. Conf. Pattern Recognit.*, Sep. 2000, pp. 314–317.

[31] F. S. Helmli and S. Scherer, "Adaptive shape from focus with an error estimation in light microscopy," in *Proc. 2nd Int. Symp. Image Signal Process. Anal., Conjunction 23rd Int. Conf. Inf. Technol. Interfaces*, Jun. 2001, pp. 188–193.
[32] X. Liu, W. H. Wang, and Y. Sun, "Dynamic evaluation of autofocusing for automated microscopic analysis of blood smear and pap smear," *J. Microsc.*, vol. 227, no. 1, pp. 15–23, 2007.
[33] M. T. Yildirim, A. Basturk, and M. E. Yuksel, "Impulse noise removal from digital images by a detail-preserving filter based on type-2 fuzzy logic," *IEEE Trans. Fuzzy Syst.*, vol. 16, no. 4, pp. 920–928, Aug. 2008.
[34] M. Kass, A. Witkin, and D. Terzopoulos, "Snakes: Active contour models," *Int. J. Comput. Vis.*, vol. 1, no. 4, pp. 321–331, Jan. 1988.
[35] L. Kiefer, "Sequential minimax search for a maximum," *Proc. Amer. Math. Soc.*, vol. 4, no. 3, pp. 502–506, Jun. 1953.
[36] Y. U. Sun, S. Duthaler, and B. J. Nelson, "Autofocusing in computer microscopy: Selecting the optimal focus algorithm," *Microsc. Res. Technique*, vol. 65, no. 3, pp. 139–149, Oct. 2004.

FERHAT SADAK received the M.Sc. degree in advanced mechanical engineering from the University of Birmingham, in 2016, where he is currently pursuing the Ph.D. degree in bio-micro robotics. His main research interests include image processing, and developing automated systems for micro injection and micro manipulation of biological systems.

MOZAFAR SAADAT received the Honour degree in mechanical engineering from the University of Surrey, U.K., and the Ph.D. degree in industrial automation from the University of Durham, U.K. He has had a range of previous experience as a manufacturing technology consultant to industry. He has obtained research funding in healthcare, electronics, manufacturing, and aerospace sectors and has published widely in leading international journals. His research interests include automation, robotic, and intelligent systems predominantly applied to healthcare and manufacturing industries.

AMIR M. HAJIYAVAND received the Honour degree in biomechanical engineering and the Ph.D. degree in medical robotics from the University of Birmingham, U.K. His main research interests include developing automated systems for micro implant, microinjection, and micromanipulation of biological systems and also developing medical technologies for infertility diagnostic and therapeutic applications.